Electronic Supplementary Information

The Effect of Side-Chain Length on the Microstructure and Processing Window of Zone-Cast Naphthalene-Based Bispentalenes

Katelyn P. Goetz[a,b], Kohei Sekine[c], Fabian Paulus[a,b], Yu Zhong[d], Daniel Roth[a], David Becker-Koch[b,e], Yvonne J. Hofstetter[b,e], Elena Michel[c], Lisa Reichert[c], Frank Rominger[c], Matthias Rudolph[c], Sven Huettner[d], Yana Vaynzof[b,e], Eva M. Herzig[f], A. Stephen K. Hashmi[c,g], Jana Zaumseil[a,b*]

[a] Institute for Physical Chemistry, Heidelberg University, Heidelberg, Germany
[b] Centre for Advanced Materials, Heidelberg University, Heidelberg, Germany
[c] Institute for Organic Chemistry, Heidelberg University, Heidelberg, Germany
[d] Organic and Hybrid Electronics, Macromolecular Chemistry I, University of Bayreuth, Bayreuth, Germany
[e] Kirchhoff Institute for Physics, Heidelberg University, Heidelberg, Germany
[f] Department of Physics, University of Bayreuth, Bayreuth, Germany
[g] Chemistry Department, Faculty of Science, King Abdulaziz University, Jeddah, Saudi Arabia

* Corresponding author email: *zaumseil@uni-heidelberg.de*

Table of Contents

1. Synthesis of NBP-Cn Molecules by Gold Catalysis

a. General Methods

Chemicals were purchased from commercial suppliers and used as delivered. Dry solvents were dispensed from the solvent purification system MB SPS-800. Deuterated solvents were bought from Euriso-Top. Reactions requiring inert conditions were carried out in flame-dried glassware under an atmosphere of nitrogen using standard Schlenk-techniques. For some reactions degassed solvents were used. To degas these solvents, nitrogen was bubbled through them for at least one hour. NMR spectra were, if not mentioned otherwise, recorded at room temperature on the following spectrometers: Bruker Avance-III-300, Bruker Avance DRX-300, Bruker-Avance DRX-500 and Bruker Avance-III-500. Chemical shifts were given in ppm and coupling constants in Hz. ^{1}H and ^{13}C spectra were calibrated in relation to deuterated solvents, namely $CDCl_3$ (7.26 ppm; 77.16 ppm). The following abbreviations were used for ^{1}H NMR spectra to indicate the signal multiplicity: s (singlet), bs (broad singlet), d (doublet), t (triplet), q (quartet), quint (quintet), sext (sextet), sept (septet) and m (multiplet) as well as combinations of them. When combinations of multiplicities are given the first character noted refers to the biggest coupling constant. All ^{13}C NMR spectra were measured with ^{1}H-decoupling. The multiplicities mentioned in these spectra [s (singlet, quaternary carbon), d (doublet, CH-group), t (triplet, CH_2-group), q (quartet, CH_3-group)] were determined by DEPT135 and HSQC spectra. Mass spectra (MS and HRMS) were determined at the chemistry department of the University of Heidelberg under the direction of Dr. J. Gross. EI^+-spectra were measured on a JOEL JMS-700 spectrometer. For ESI^+-spectra a Bruker ApexQu FT-ICR-MS spectrometer was applied. Infrared Spectroscopy (IR) was processed on an FT-IR Bruker (IF528), IR Perkin Elmer (283) or FT-IR Bruker Vector 22. The solvent or matrix is denoted in brackets. For the most significant bands the wave number $\tilde{\nu}$ (cm^{-1}) is given. X-ray crystal structure analyses were measured at the chemistry department of the University of Heidelberg under the direction of Dr. F. Rominger on a Bruker Smart CCD or Bruker APEX-II CCD instrument using Mo-Kα-radiation. Diffraction intensities were corrected for Lorentz and polarization effects. An empirical absorption correction was applied using SADABS based on the Laue symmetry of reciprocal space. Heavy atom diffractions were solved by direct methods and refined against F2 with full matrix least square algorithm. Hydrogen atoms were either isotropically refined or calculated. The structures were solved and refined by Dr. F. Rominger using the SHELXTL software package. Gas Chromatography / Mass Spectrometry (GC/MS) spectra were measured on two different hardware systems: 1. HP 5972 Mass Selective Detector,

coupled with a HP 5890 SERIES II plus gas chromatograph. 2. Agilent 5975C Mass Selective Detector, coupled with an Agilent 7890A gas chromatograph. In both cases, as a capillary column, an OPTIMA 5 cross-linked Methyl Silicone column (30 m x 0.32 mm, 0.25 μm) was employed and helium was used as the carrier gas. Melting Points were measured in open glass capillaries in a Büchi melting point apparatus (according to Dr. Tottoli) and were not corrected. Flash Column Chromatography was accomplished using Silica gel 60 (0.063-0.200 mm / 230 mesh ASTM) purchased from Sigma-Aldrich or aluminium oxide (neutral or basic) purchased from Macherey-Nagel. As eluents, mixtures of petroleum ether (PE), ethyl acetate (EA), dichloromethane (DCM) and diethylether (Et_2O) were used. Analytical Thin Layer Chromatography (TLC) was carried out on precoated Macherey-Nagel POLYGRAM® SIL G/UV254 or POLYGRAM® ALOX N/UV254 plastic sheets. Detection was accomplished using UV-light (254 nm), $KMnO_4$ (in 1.5M Na_2CO_3 (aq.)), molybdatophosphoric acid (5 % in ethanol), vanillin/H_2SO_4 (in ethanol) or anisaldehyde/HOAc (in ethanol). IUPAC names of the compounds described in the experimental section were determined with the program ACDLabs 12.0®.

b. Synthesis of Starting Materials 1-Cn

Tetrakis(arylethynyl)naphthalenes **1-Cn** were synthesized according to the previous report[S1] by Sonogashira-coupling reaction (Scheme S1). 3,6-dibromo-2,7-bis(trifluoromethane-sulfonyloxy)naphthalene was synthesized as reported. [S2] The analytical data of **1-C5** is in the previous literature.[S3]

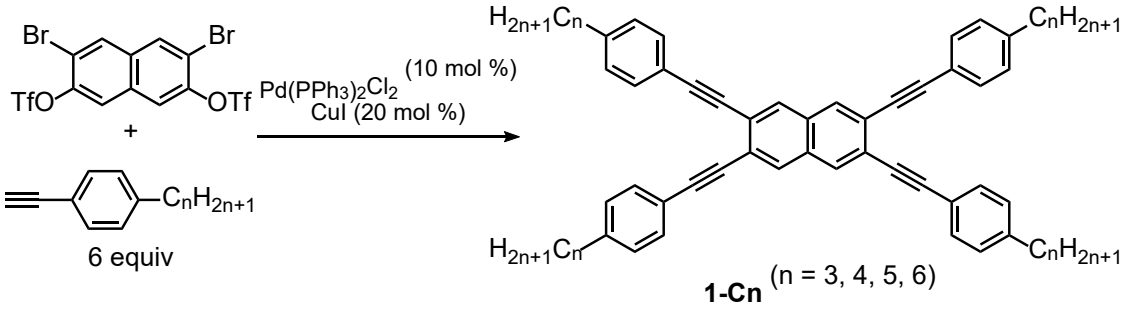

Scheme S1. Synthesis of 2,3,6,7-tetrakis(arylethynyl)naphthalene **1-C6**, **1-C5**, **1-C4**, **1-C3**.

2,3,6,7-tetrakis((4-hexylphenyl)ethynyl)naphthalene(**1-C6**):

1-C6 was synthesized by the same method as **1-C8**.

72% yield; Pale yellow solid; **m.p.** 186–186.6 °C; **IR** (ATR): 2953, 2925, 2855, 2212, 1514, 1468, 912, 826 cm^{-1}; **^{1}H NMR** (400 MHz, $CDCl_3$): δ = 0.90 (t, *J* = 6.9 Hz, 12H), 1.30–1.36 (m, 24H), 1.63 (quint, *J* = 7.5 Hz, 8H), 2.63 (t, *J* = 7.7 Hz, 8H), 7.18 (d, *J* = 8.1 Hz, 4H), 7.52 (d, *J* = 8.1 Hz, 4H), 7.97 (s, 4H); **^{13}C NMR** (150 MHz, $CDCl_3$): δ =14.4(q, 4C), 22.9(t, 4C), 29.3(t, 4C), 31.5(t, 4C), 32.0(t, 4C), 36.3(t, 4C), 88.1(s, 4C), 94.7(s, 4C), 120.6(s, 4C), 124.2(s, 4C), 128.8(d, 8C), 131.2(d, 8C), 131.4(s, 2C), 132.0(d, 4C), 144.1(s, 4C); **HRMS** (MALDI): $[C_{66}H_{72}]^+$, calcd.:864.5629, found: 864.5599.

2,3,6,7-tetrakis((4-butylphenyl)ethynyl)naphthalene(**1-C4**) :

The corresponding alkyne (6 equiv, 4.32 mmol) was added to the solution of $Pd(PPh_3)_2Cl_2$ (10 mol %, 0.43 mmol), CuI (20 mol %, 0.86 mmol), and 3,6-dibromo-2,7-bis(trifluoromethanesulfonyloxy)naphthalene (1 equiv, 0.72 mmol) in degassed ^{i}Pr$_2$NH (15 mL)/THF (15 mL). The solution was heated at 50 °C. After stirred overnight, the reaction mixture was filtered with a short pad of Celite and silica gel and washed with PE/DCM to remove side products. The crude mixture was purified by column chromatography (SiO_2, eluent: PE/DCM) to afford the desired compound (479 mg, 0.636 mmol).

88% yield; Pale yellow solid; **m.p.** 179–180 °C; **IR** (ATR): 2957, 2928, 2854, 2210, 1576, 1512, 1466, 1376, 1300, 1088, 1019, 910, 820, 636 cm^{-1}; **^{1}H NMR** (600 MHz, $CDCl_3$): δ = 0.94 (t, *J* = 7.4 Hz, 12H), 1.36 (dt, *J* = 7.4, 7.4 Hz, 8H), 1.60-1.64 (m, 8H), 2.64 (t, *J* = 7.7 Hz, 8H), 7.18 (d, *J* = 8.2 Hz, 8H), 7.52 (d, *J* = 8.1 Hz, 8H), 7.98 (s, 4H); **^{13}C NMR** (125 MHz, $CDCl_3$): δ = 14.1 (q, 4C), 22.5 (t, 4C), 33.5 (t, 4C), 35.8 (t, 4C), 87.9 (s, 4C), 94.5 (s, 4C), 120.5 (s, 4C), 124.0 (s, 4C), 128.7 (d, 8C), 131.1 (d, 8C), 131.3 (s, 2C), 131.9 (d, 4C), 143.9 (s, 4C); **HRMS** (MALDI): $[C_{58}H_{48}]^+$, calcd.: 752.4382, found: 752.549.

2,3,6,7-tetrakis((4-butylphenyl)ethynyl)naphthalene(**1-C3**) :

The corresponding alkyne (6 equiv, 3.6 mmol) was added to the solution of $Pd(PPh_3)_2Cl_2$ (10 mol %, 0.06 mmol), CuI (20 mol %, 0.12 mmol), and 3,6-dibromo-2,7-bis(trifluoromethanesulfonyloxy)naphthalene (1 equiv, 0.6 mmol) in degassed $^{i}Pr_2NH$ (3 mL)/THF (3 mL). The solution was heated at 60 °C. After stirred for 12 h, the reaction mixture was filtered with a short pad of Celite and silica gel and washed with PE/DCM to remove side products. The short pad was washed with hot $CHCl_3$ and the solvent was removed under reduced pressure to give the desired compound (291 mg, 0.418 mmol).

70% yield; Pale yellow solid; **m.p.** 215–216 °C; **IR** (ATR): 3031, 2964, 2865, 2214, 1578, 1514, 1091, 912, 838, 759 cm^{-1}; **^{1}H NMR** (300 MHz, $CDCl_3$): δ = 0.89 (t, *J* = 7.3 Hz, 12H), 1.54–1.66 (m, 8H), 2.55 (t, *J* = 7.6 Hz, 8H), 7.11 (d, *J* = 8.2 Hz, 4H), 7.46 (d, *J* = 8.2 Hz, 4H), 7.91 (s, 4H); **^{13}C NMR** (100 MHz, $CDCl_3$): δ = 13.6(q, 4C), 24.1(t, 4C), 38.0(t, 4C), 87.8(s, 4C), 94.4(s, 4C), 120.5(s, 4C), 124.1(s, 4C), 128.5(d, 8C), 130.9(d, 8C), 131.2(s, 2C), 131.7(d, 4C), 143.4(s, 4C); **HRMS** (MALDI): $[C_{54}H_{48}]^+$, calcd.:696.3751, found:696.374.

c. Gold-catalyzed Reaction for NBP-Cn Molecules

General Procedure:

In a vial, (IPr)AuCl (10 mol %) and $AgNTf_2$ (10 mol %) were dissolved in dry dichloromethane (0.5 mL). After stirring for 5 min, the substrate (1 equiv, 0.05 mmol) in the solvent (1.0 mL) was added. The vial was closed properly and the reaction mixture was stirred at room temperature until complete conversion was detected by TLC. Then, the crude product was purified by flash column chromatography (SiO_2, eluent: PE/DCM) to yield the naphthalene-based pentalene (**NBP-Cn**).

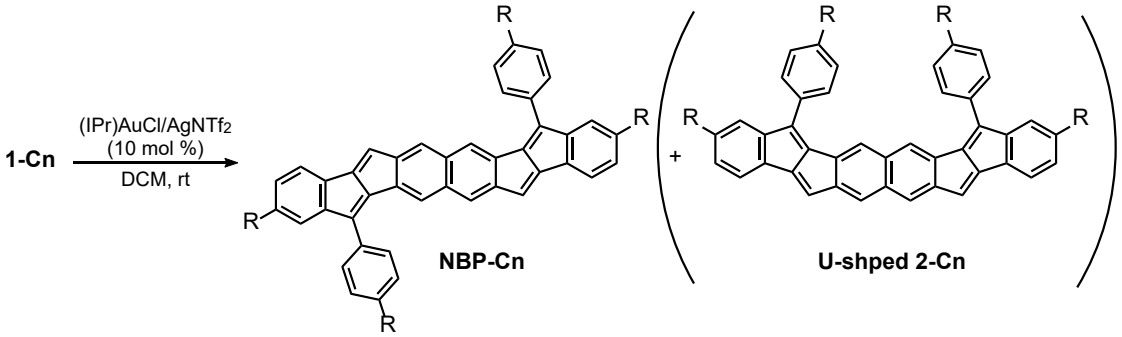

The analytical data of **NBP-C5** is in the previous literature.[S3]

S-shaped bispentalenes **NBP-C6** was synthesized by **GP**. The crude product was purified by flash column chromatography (SiO_2, eluent: PE/DCM = 12:1) to give **NBP-C6** and **U-shape 2-C6** in 47% and 42% isolated yields, respectively.

NBP-C6: 47% isolated yield; Purple solid; **m.p.** 186.9–187.8 °C; **IR** (ATR): 3063, 2922, 2854, 1596, 1439, 1129, 898, 834 cm^{-1}; **UV-Vis** (DCM): λ (log ε) = 273 (4.69), 321 (4.72), 341 (4.72), 341 (4.8), 361 (4.97), 376 (5.04), 477 (4.22), 509 (4.51), 548 nm (4.62); **^{1}H NMR** (600 MHz, $CDCl_3$): δ = 0.88 (t, *J* = 6.8 Hz, 6H), 0.93 (t, *J* = 6.9 Hz, 6H), 1.28–1.31 (m, 8H), 1.35–1.40 (m, 8H), 1.43–1.45 (m, 4H), 1.53–1.58 (m, 4H), 1.70–1.75 (m, 4H), 2.49 (t, *J* = 7.8 Hz, 4H), 2.73 (t, *J* = 7.9 Hz, 4H), 6.57 (s, 2H), 6.80 (d, *J* = 7.5 Hz, 2H), 6.94 (s, 2H), 7.00 (s, 2H), 7.16 (d, *J* = 7.4 Hz, 2H), 7.34 (s, 2H), 7.36 (d, *J* = 7.9 Hz, 4H), 7.62 (d, *J* = 7.9 Hz, 4H); **^{13}C NMR** (150 MHz, $CDCl_3$): δ = 14.4 (q), 14.5(q), 22.9(t), 23.0(t), 29.3(t), 29.5(t), 31.7(t), 31.8(t), 32.0(t), 32.1(t), 36.3(t), 36.5(t), 121.9(d), 122.4(d), 123.0(d), 123.3(d), 124.6(d), 127.1(d), 128.7(d), 129.0(d), 131.8(s), 132.3(s), 133.2(s), 134.2(s), 139.2(s), 142.7(s), 143.7(s), 144.0(s), 148.6(s), 150.37(s), 150.41(s); **HRMS** (MALDI): $[C_{66}H_{72}]^+$, calcd.:864.5629, found:864.5640.

S-shaped bispentalenes **NBP-C4** was synthesized by **GP**. The crude product was purified by flash column chromatography (SiO_2, eluent: PE:DCM = 10:1) to give **NBP-C4** and **U-shape 2-C4** in 42% and 40% isolated yields, respectively.

NBP-C4: 42% isolated yield; Purple solid; **m.p.** 271–272 °C; **IR** (ATR): 2953, 2925, 2855, 1738, 1594, 1439, 1345, 1183, 1133, 929, 814 cm^{-1}; **UV-Vis** (DCM): λ (log ε) = 275 (4.60), 323 (4.68), 343 (4.76), 360 (4.94), 376 (5.01), 476 (4.14), 508 (4.47), 548 nm (4.60); **^{1}H NMR** (600 MHz, $CDCl_3$): δ = 0.84 (t, *J* = 7.4 Hz, 6H), 0.98 (t, *J* = 7.4 Hz, 6H), 1.24–1.30 (m, 4H), 1.36–1.42 (m, 4H), 1.44–1.50 (m, 4H), 1.62–1.67 (m, 4H), 2.42 (t, *J* = 7.8 Hz, 4H), 2.66 (t, *J* = 7.8 Hz, 4H), 6.49 (s, 2H), 6.72 (d, *J* = 7.5 Hz, 2H), 6.86 (s, 2H), 6.92 (s, 2H), 7.08 (d, *J* = 7.5 Hz, 2H), 7.27 (s, 2H), 7.29 (d, *J* = 7.9 Hz, 4H), 7.54 (d, *J* = 7.9 Hz, 4H); **^{13}C NMR** (150 MHz, $CDCl_3$): δ = 14.1(q, 2C), 14.2(q, 2C), 22.5(t, 2C), 22.7(t, 2C), 33.7(t, 2C), 33.8(t, 2C), 35.9(t, 2C), 36.1(t, 2C), 121.8(d, 2C), 122.2(d, 2C), 122.8(d, 2C), 123.1(d, 2C), 124.4(d, 2C), 126.9(d, 2C), 128.5(d, 4C), 128.9(d, 4C), 131.6(s, 2C), 132.1(s, 2C), 133.0(s, 2C), 134.0(s, 2C), 139.0(s, 2C), 142.5(s, 2C), 143.5(s, 2C), 143.8(s, 2C), 148.4(s, 2C), 150.2(s, 2C), 150.24(s, 2C); **HRMS** (MALDI): $[C_{58}H_{57}]^+$, calcd.:753.4455, found:753.4453.

S-shaped bispentalenes **NBP-C3** was synthesized by GP. The crude product was purified by flash column chromatography (SiO_2, eluent: PE:DCM = 8:1) to give **NBP-C3** in 28% isolated yield and a mixture of **NBP-C3** and **U-shaped 2-C3**.

NBP-C3: 28% isolated yield; Purple solid; **m.p.** 286–297 °C; **IR** (ATR): 3028, 2956, 2868, 1715, 1594, 1461, 1345, 1094, 965, 807 cm^{-1}; **UV-Vis** (DCM): λ (log ε) = 274 (4.56), 318 (4.62), 339 (4.74), 359 (4.94), 375 (5.01), 475 (4.10), 507 (4.45), 547 nm (4.62); **^{1}H NMR** (300 MHz, $CDCl_3$): δ = 0.86 (t, *J* = 7.3 Hz, 6H), 0.98 (t, *J* = 7.3 Hz, 6H), 1.49–1.59 (m, 8H), 1.64–1.76 (m, 8H), 2.41 (t, *J* = 7.6 Hz, 4H), 2.64 (t, *J* = 7.7 Hz, 4H), 6.50 (s, 2H), 6.73 (d, *J* = 7.3 Hz, 2H), 6.87 (s, 2H), 6.93 (s, 2H), 7.09 (d, *J* = 7.5 Hz, 2H), 7.28–7.30 (m, 6H), 7.55 (d, *J* = 8.0 Hz, 4H); **^{13}C NMR** (100 MHz, $CDCl_3$): δ = 13.8(q), 14.0(q), 24.4(t), 24.5(t), 38.1(t), 38.3(t), 121.6(d), 122.1(d), 122.7(d), 123.0(d), 124.3(d), 126.8(d), 128.4(d), 128.8(d), 131.6(s), 132.0(s), 132.9(s), 133.9(s), 138.9(s), 142.4(s), 143.2(s), 143.4(s), 148.3(s), 150.1(s), 150.1(s); **HRMS** (MALDI): $[C_{54}H_{48}]^+$, calcd.:696.3751, found:696.376.

d. NMR spectra

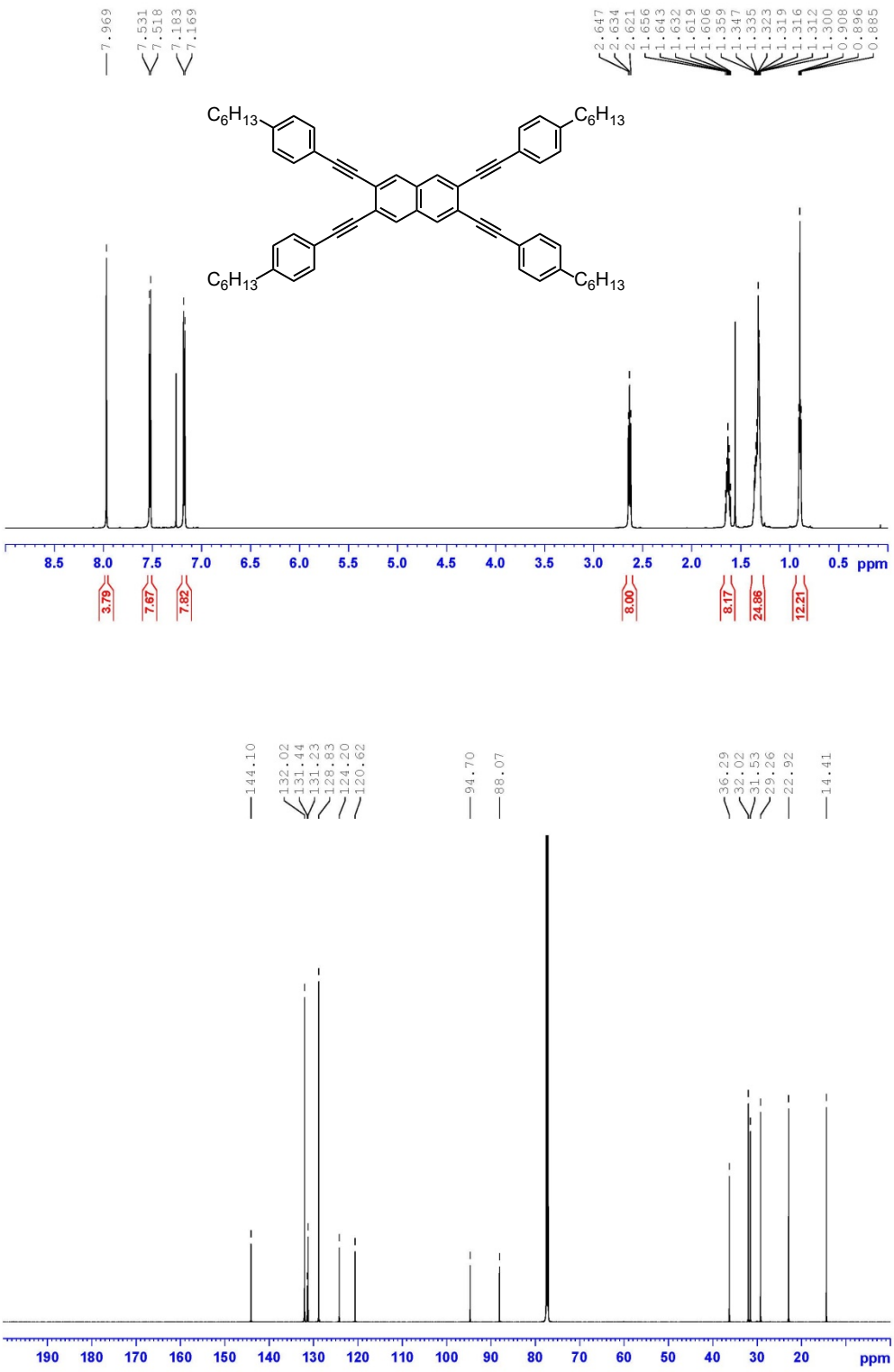

Figure S1. ^{1}H NMR and ^{13}C NMR in $CDCl_3$ (**1-C6**)

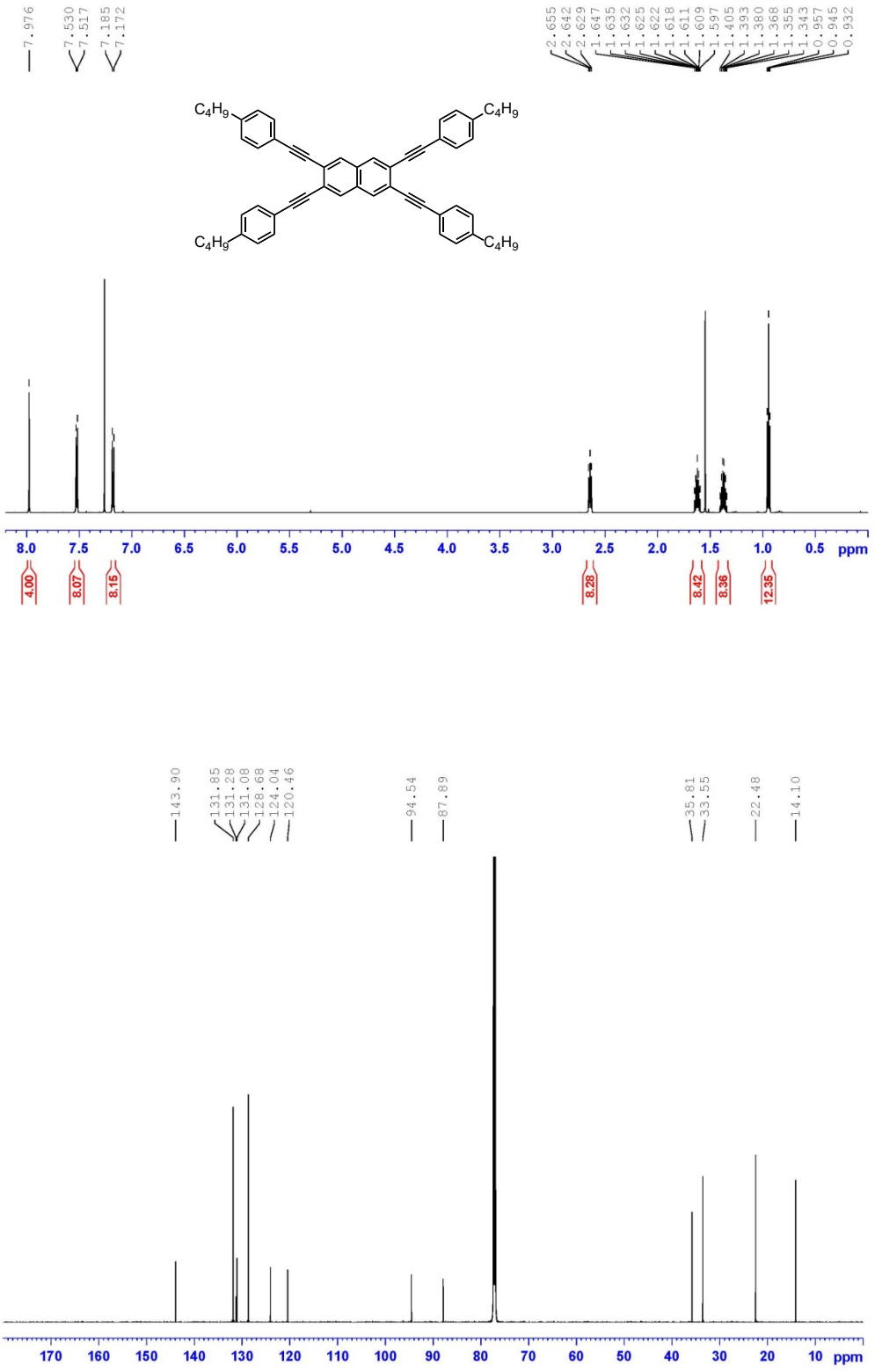

Figure S2. ^{1}H NMR and ^{13}C NMR in $CDCl_3$ (**1-C4**)

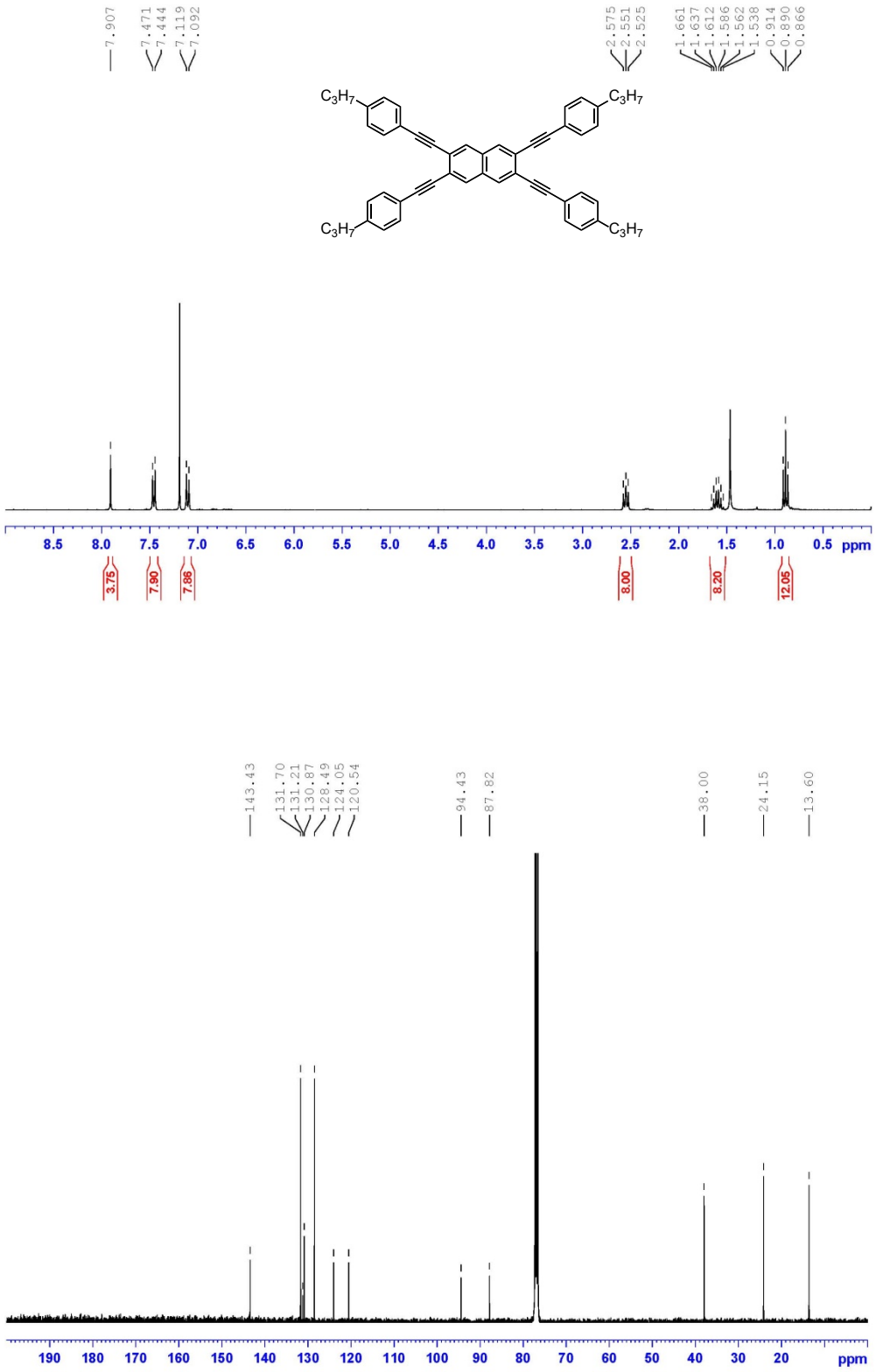

Figure S3. ^{1}H NMR and ^{13}C NMR in $CDCl_3$ ((**1-C3**)

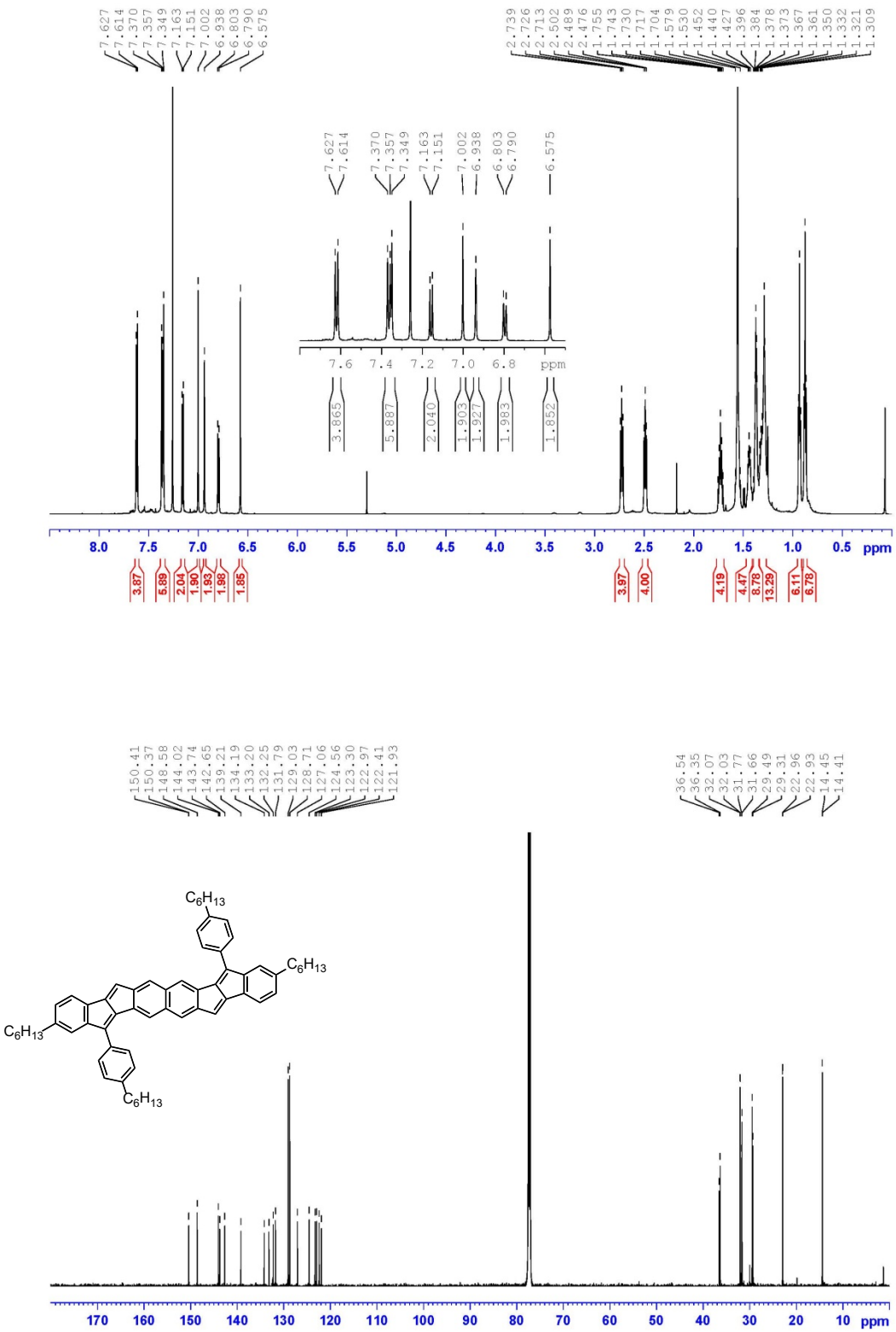

Figure S4. ^{1}H NMR and ^{13}C NMR in $CDCl_3$ (**NBP-C6**)

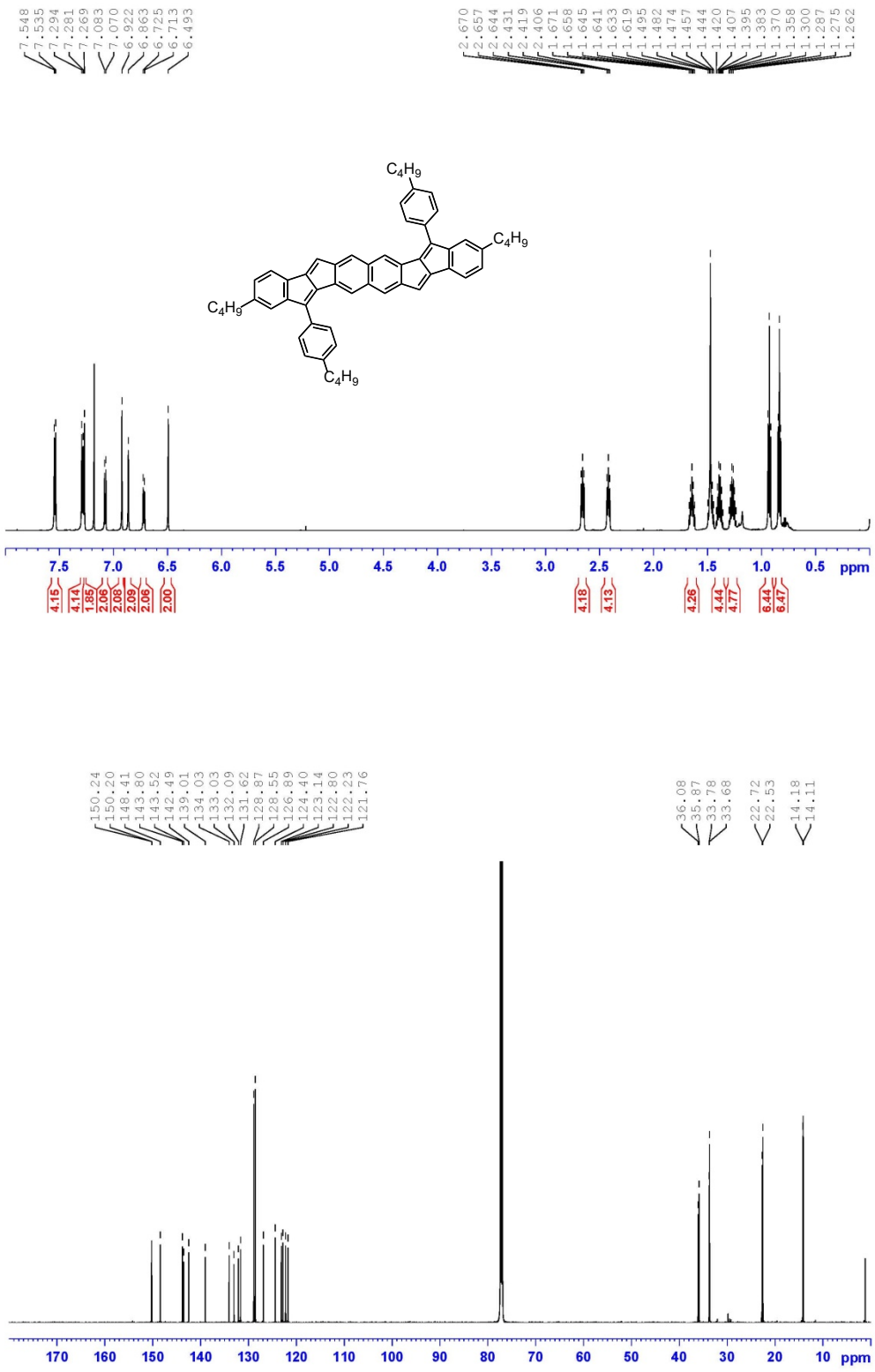

Figure S5. ^{1}H NMR and ^{13}C NMR in $CDCl_3$ (**NBP-C4**)

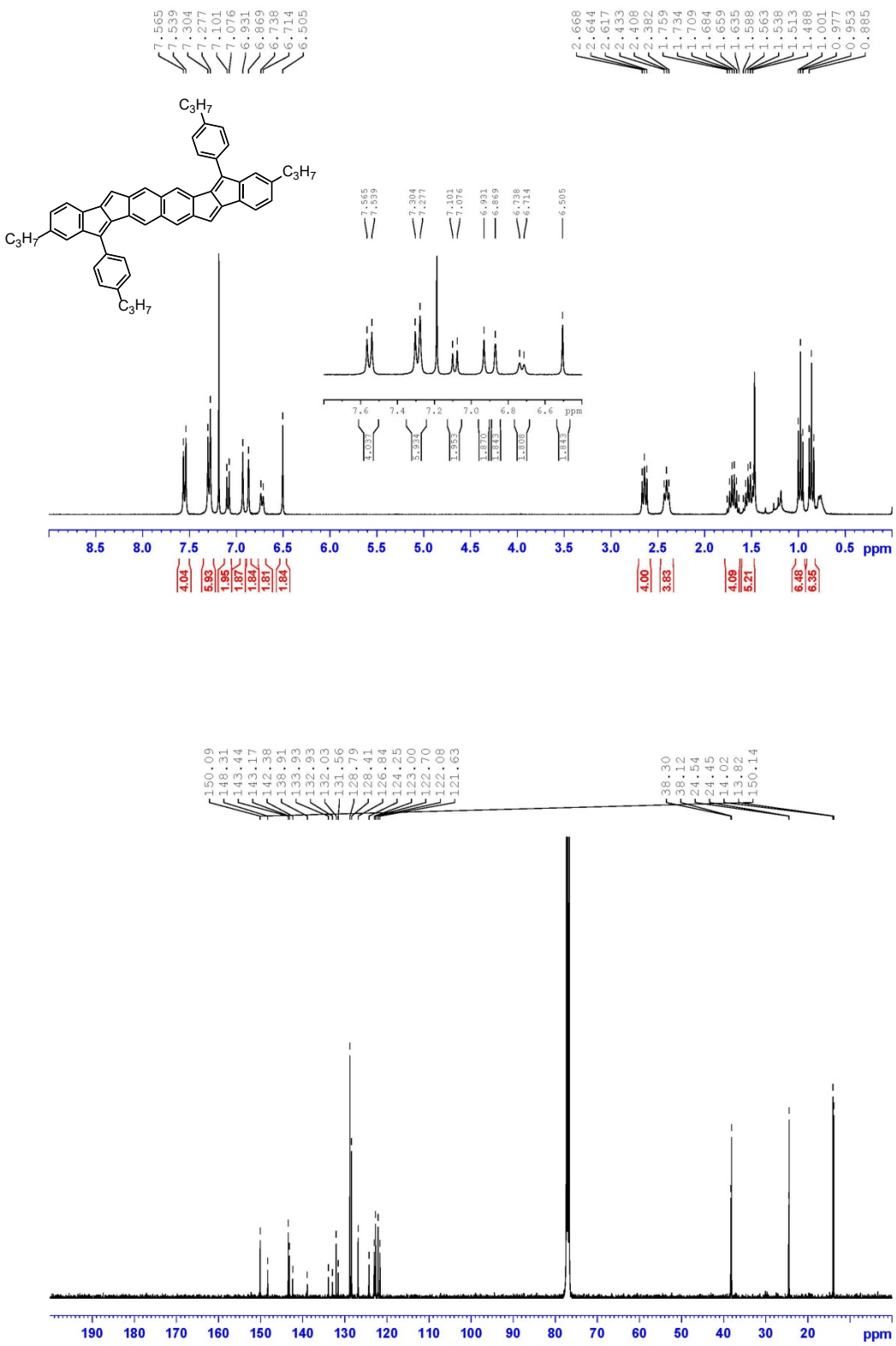

Figure S6. ^{1}H NMR and ^{13}C NMR in $CDCl_3$ (**NBP-C3**)

2. Differential Scanning Calorimetry

Differential scanning calorimetry measurements were performed in hermetically sealed aluminum pans at a scanning rate of 10 K/min using a TA Instruments DSC250. The orientation of the plot is exothermic up. The melting point decreases with increasing chain length.

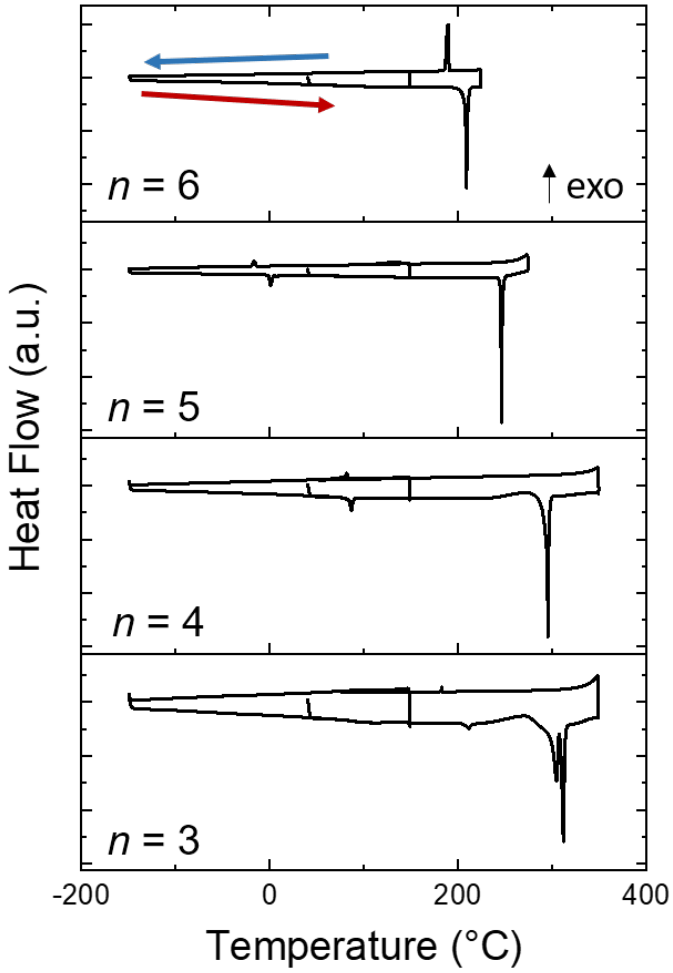

Figure S7. DSC measurements of each NBP-C*n*. The melting point decreases with increasing chain length.

3. Single Crystal X-ray Diffraction

The structures were refined using standard procedures. Diffraction intensities were corrected for Lorentz and polarization effects, and an empirical absorption correction was applied based on the Laue symmetry of the reciprocal space. Heavy atom diffractions were solved by direct methods and refined against F^2 with a full matrix least square algorithm. Hydrogen atoms were considered at calculated positions. CCDC 1941693 (n = 3), 1941694 (n = 4), and 1851125 (n = 5) contain the supplementary crystallographic data for this paper. These data can be obtained free of charge from The Cambridge Crystallographic Data Centre via https://www.ccdc.cam.ac.uk/structures/.

4. AFM Height Profiles of NBP-C*n*

The height profiles for the NBP-C*n* films (Fig. S8) are shown for the films in Fig. 3. The film thickness increases from 10 nm (0.4 mm/s) to 40-60 nm (0.2 mm/s) to 100-200 nm (0.05 mm/s) with decreasing casting speed. The variation in ribbon height above the minimum point of the AFM image is given by Δt. Slow-cast films show larger variations in ribbon height.

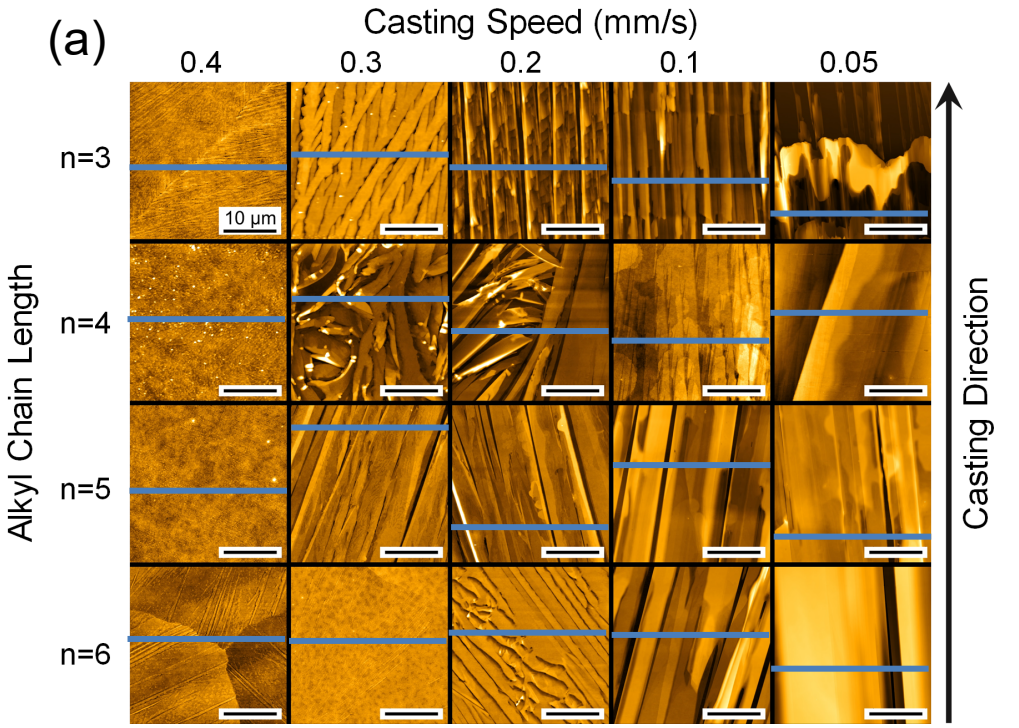

Figure S8. Height profiles of the AFM images from the main text Fig. 3, with the line cuts shown in (a). The profiles for the $n = 3$ compound are shown in (b), the profiles for the $n = 4$ compound are shown in (c), $n = 5$ in (d), and $n = 6$ in (e).

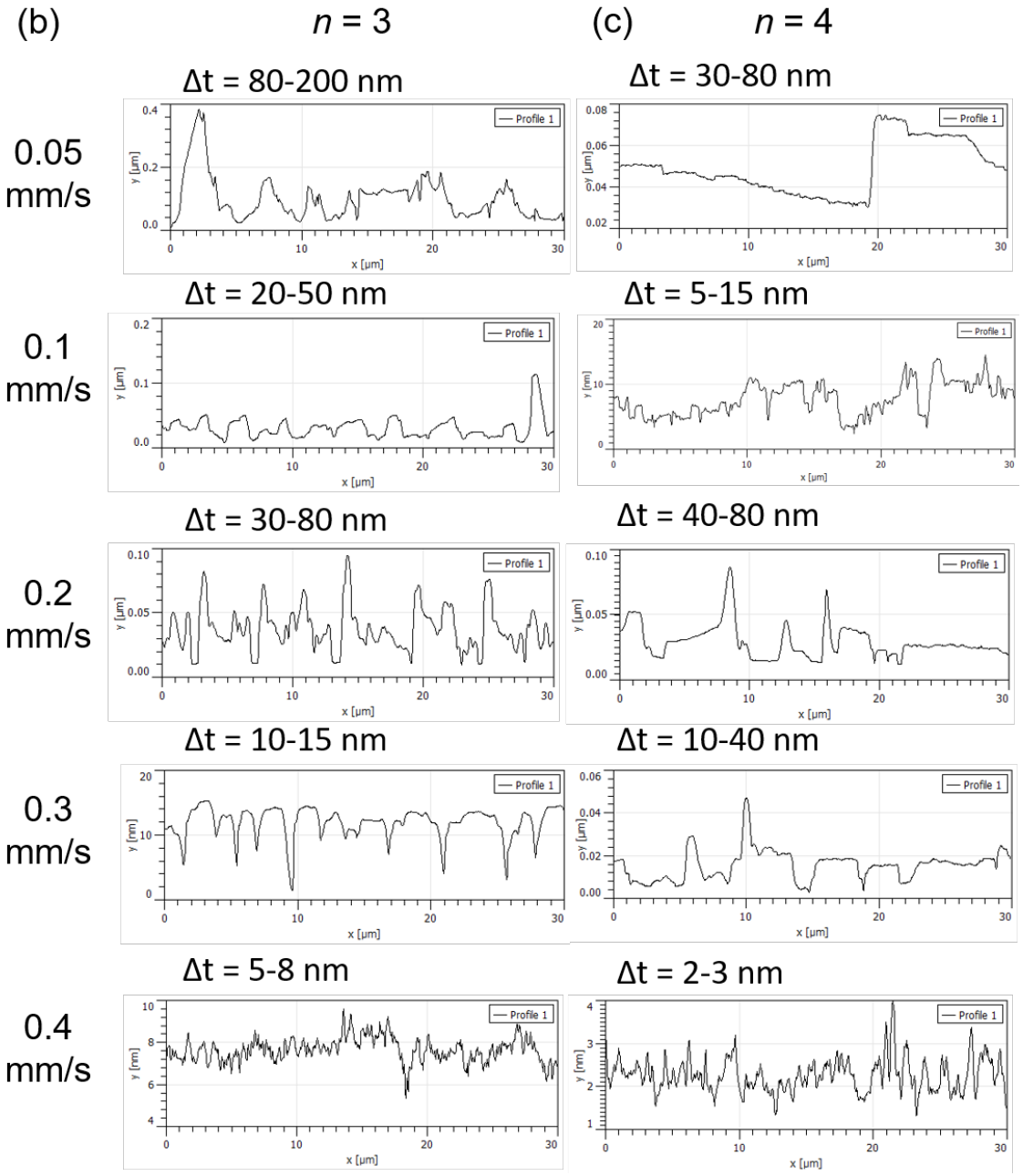
(b) n = 3
(c) n = 4
0.05 mm/s
Δt = 80-200 nm
Δt = 30-80 nm
0.1 mm/s
Δt = 20-50 nm
Δt = 5-15 nm
0.2 mm/s
Δt = 30-80 nm
Δt = 40-80 nm
0.3 mm/s
Δt = 10-15 nm
Δt = 10-40 nm
0.4 mm/s
Δt = 5-8 nm
Δt = 2-3 nm
Profile 1
x [µm]
y [µm]
y [nm]

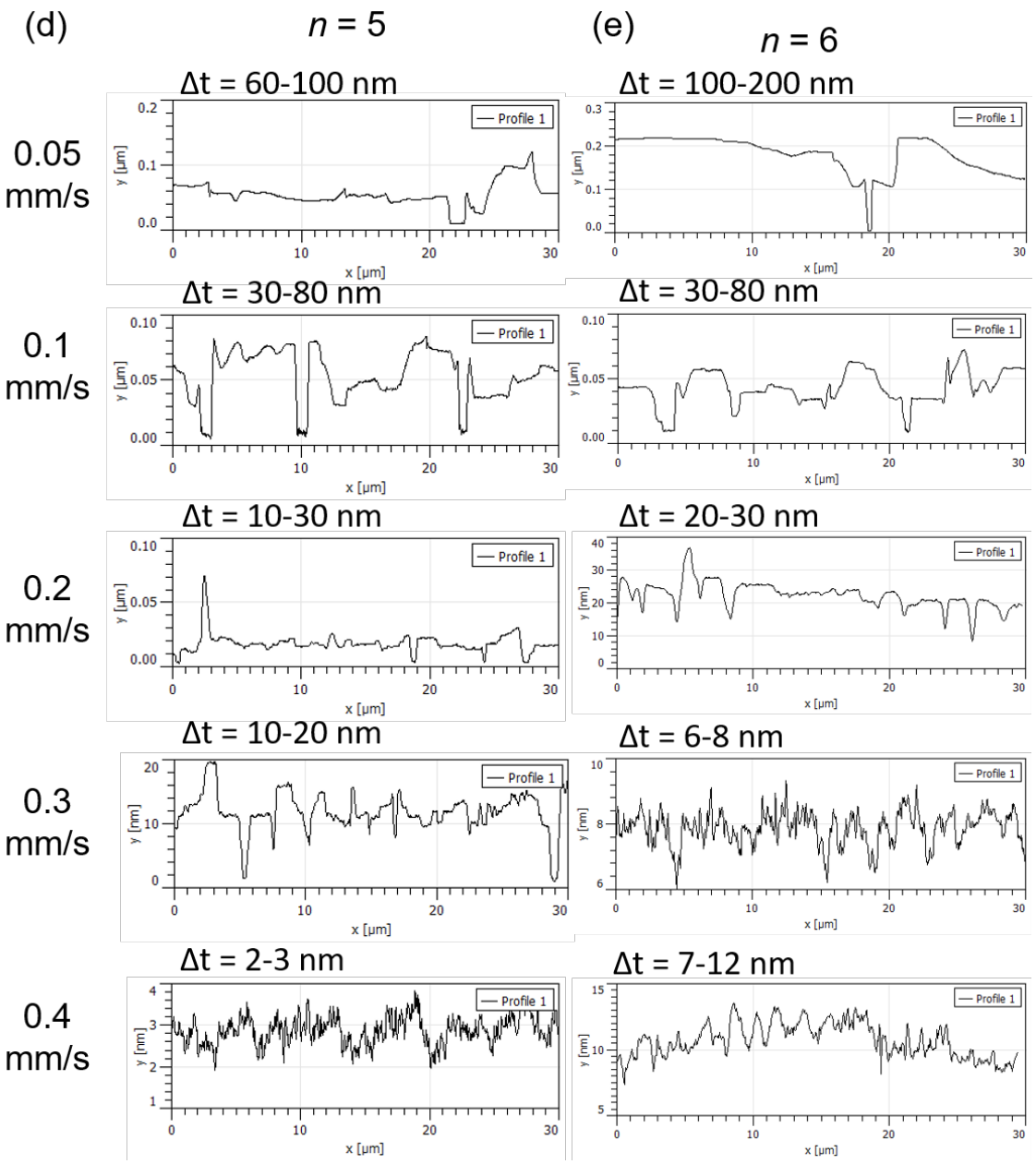
(d)
n = 5
(e)
n = 6
0.05 mm/s
Δt = 60-100 nm
Δt = 100-200 nm
0.1 mm/s
Δt = 30-80 nm
Δt = 30-80 nm
0.2 mm/s
Δt = 10-30 nm
Δt = 20-30 nm
0.3 mm/s
Δt = 10-20 nm
Δt = 6-8 nm
0.4 mm/s
Δt = 2-3 nm
Δt = 7-12 nm
Profile 1
x [µm]
y [µm]
y [nm]

5. Thin-Films with Long Alkyl Side-Chain Length (*n* = 8)

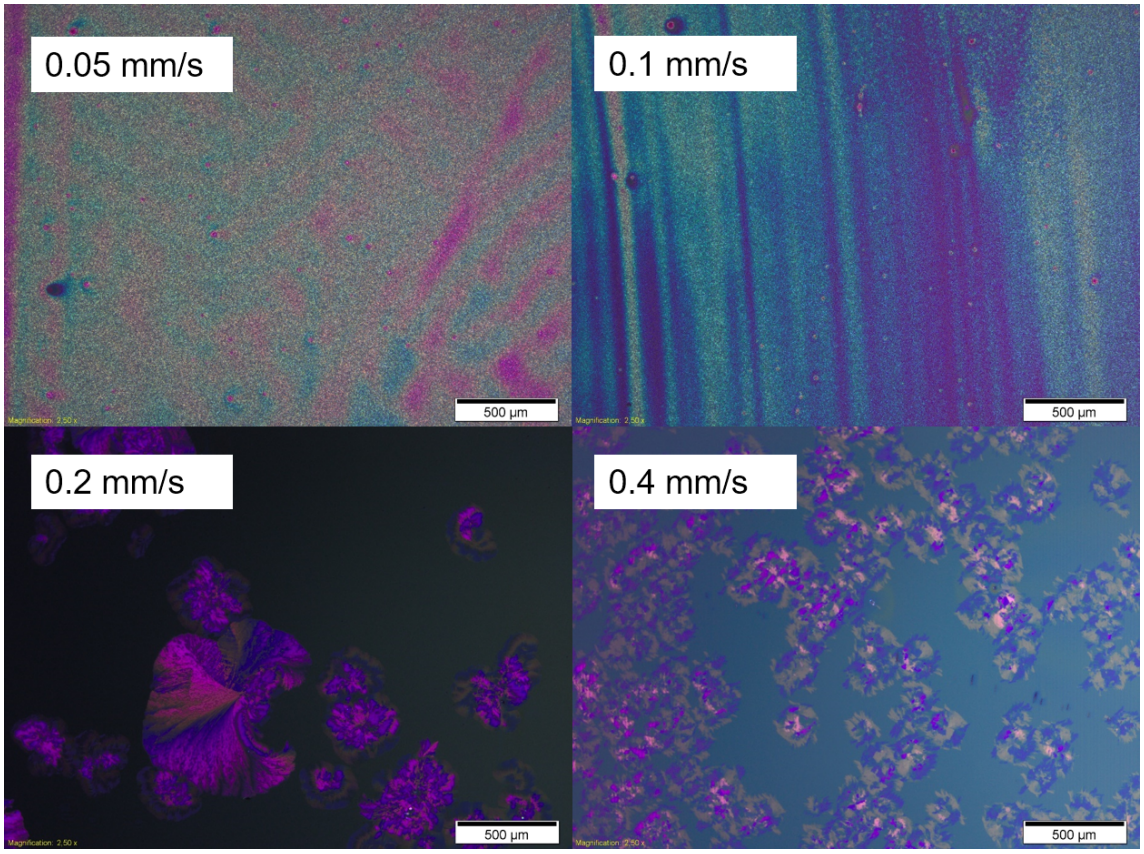

Figure S9. Optical microscopy of films of NBP-C8 cast at varying speeds. At slow speeds, very small grains are observed; at fast speeds, islands with some crystalline regions are observed, but interspersed by regions of no discernably crystalline features.

6. Current-Voltage Characteristics of NBP-C*n* Thin Film Transistors

The electrical characteristics for all NBP-C*n* are shown here, including the gate-voltage dependence of the charge-carrier mobility. The field-effect mobility (μ) was calculated using the gradual channel approximation in the saturation and linear regimes (eq. 1, eq. 2 respectively), and the reliability factor[4] was calculated based on equations 3, 4. The value for μ_{sat} was calculated over the range of -50 V - -60 V for the purposes of comparison. We note that the reliability factor primarily scales with the threshold-voltage shift, as the devices are not on for the entire range of the I_D at 0 V maximum (-60 V) I_D. Here, L is the channel length, W is the channel width, C_i is the capacitance per unit area of the dielectric, V_{DS} is the source-drain voltage, V_{GS} is the gate-source voltage, I_D is the drain current.

Eq. 1
$$\mu_{sat} = \frac{2L}{WC_i}\left(\frac{\partial\sqrt{I_D}}{\partial V_{GS}}\right)^2$$

Eq. 2
$$\mu_{lin} = \frac{L}{V_{DS}WC_i}\frac{\partial I_D}{\partial V_{GS}}$$

Eq. 3
$$r_{lin} = \left(\frac{|I_D|^{max} - |I_D^0|}{|V_{GS}|^{max}}\right) \Big/ \left(\frac{|V_{DS}|WC_i}{L}\mu_{lin}\right)$$

Eq. 4
$$r_{sat} = \left(\frac{\sqrt{|I_D|^{max}} - \sqrt{|I_D^0|}}{|V_{GS}|^{max}}\right)^2 \Big/ \left(\frac{WC_i}{2L}\mu_{sat}\right)$$

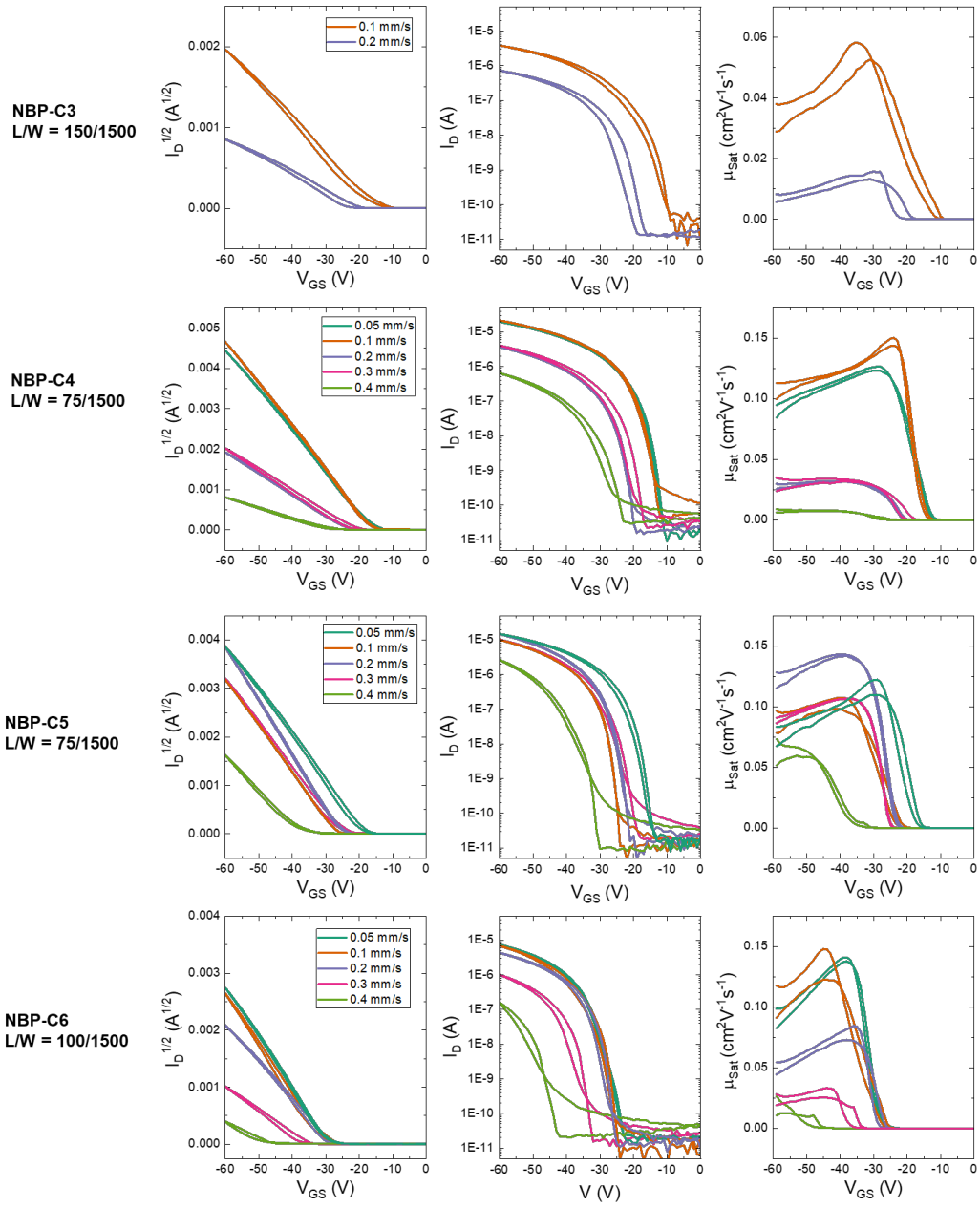

Figure S10. The square-root current-voltage plots from which mobility is extracted, the current-voltage plots, and the gate-source voltage dependence of the charge-carrier mobility.

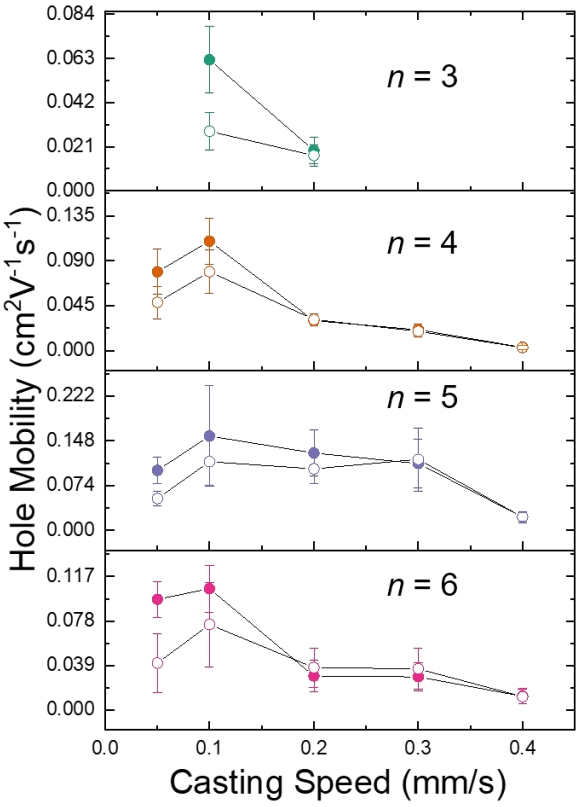

Figure S11. Linear (open circles) and saturation (closed circles) mobility for each NBP-C*n*. They are not largely different, indicating the low impact of contact resistance on the measurement and justifying the use of the gradual channel approximation model.

Table S1. Summary of the electrical characteristics for all NBP-C*n* compounds, including the reliability (r)[4], the value for which is given by eqs. 3,4.

n	v_{Cast} (mm/s)	μ_{Sat} ($cm^2V^{-1}s^{-1}$)	μ_{Lin} ($cm^2V^{-1}s^{-1}$)	V_T (V)	r_{sat}	r_{lin}
3	**0.05**	x	x	x	x	x
	0.1	0.06 ± 0.016	0.03 ± 0.009	-20 ± 4	0.42 ± 0.09	0.66 ± 0.07
	0.2	0.02 ± 0.006	0.02 ± 0.005	-19 ± 5	0.42 ± 0.12	0.48 ± 0.09
	0.3	x	x	x	x	x
	0.4	x	x	x	x	x
4	**0.05**	0.08 ± 0.02	0.05 ± 0.02	-15 ± 3	0.53 ± 0.07	0.80 ± 0.08
	0.1	0.11 ± 0.02	0.08 ± 0.02	-15 ± 3	0.56 ± 0.08	0.79 ± 0.06
	0.2	0.03 ± 0.003	0.03 ± 0.006	-17 ± 3	0.43 ± 0.11	0.56 ± 0.08
	0.3	0.02 ± 0.006	0.02 ± 0.006	-22 ± 3	0.33 ± 0.07	0.54 ± 0.07
	0.4	0.003 ± 0.0026	0.003 ± 0.002	-33 ± 5	0.20 ± 0.08	0.35 ± 0.13
5	**0.05**	0.10 ± 0.02	0.05 ± 0.01	-15 ± 4	0.56 ± 0.09	0.71 ± 0.06
	0.1	0.09 ± 0.02	0.07 ± 0.02	-18 ± 2	0.34 ± 0.14	0.53 ± 0.09
	0.2	0.13 ± 0.05	0.10 ± 0.02	-19 ± 4	0.45 ± 0.10	0.62 ± 0.07
	0.3	0.11 ± 0.04	0.11 ± 0.05	-34 ± 6	0.19 ± 0.07	0.37 ± 0.11
	0.4	0.02 ± 0.009	0.02 ± 0.007	-38 ± 2	0.13 ± 0.02	0.30 ± 0.05
6	**0.05**	0.09 ± 0.02	0.04±0.03	-28 ± 2	0.27 ± 0.03	0.42 ± 0.05
	0.1	0.11 ± 0.04	0.07±0.04	-27 ± 3	0.29 ± 0.05	0.50 ± 0.06
	0.2	0.03 ± 0.01	0.04±0.02	-26 ± 3	0.32 ± 0.06	0.39 ± 0.03
	0.3	0.03 ± 0.007	0.04±0.02	-33 ± 3	0.20 ± 0.04	0.34 ± 0.02
	0.4	0.01 ± 0.007	0.01±0.006	-42 ± 4	0.09 ± 0.04	0.22 ± 0.07

7. Ultraviolet Photoelectron Spectroscopy of the NBP-C*n* Molecules

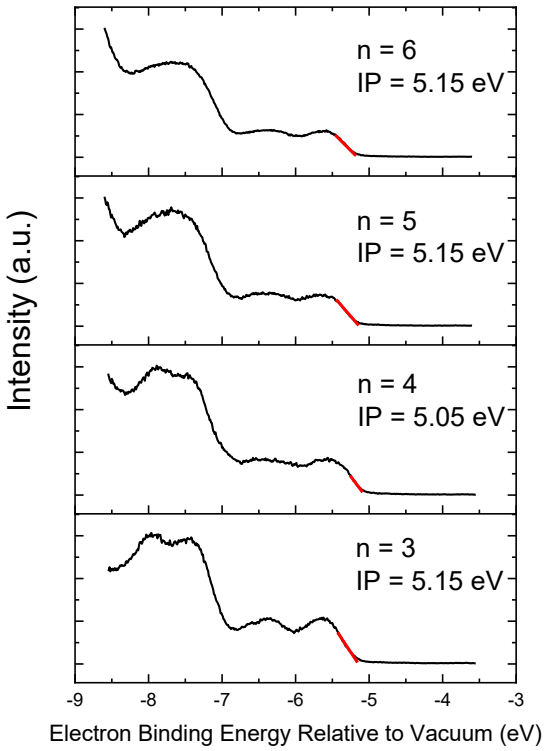

Figure S12. Ultraviolet photoelectron spectroscopy of NBP-C*n* molecules, and corresponding ionization potentials (IP).

8. XRD and GIWAXS: Additional Information

Lattice parameters extracted from the GIWAXS and single crystal XRD measurements are tabulated here. Note that the single crystal structures for n = 3 and n = 4 contained solvent molecules, that the GIWAXS was performed at room temperature, and the single crystal measurement was performed at 200 K for n = 3,4 and 100 K for n = 5.

Table S2. Comparison of lattice parameters extracted from single crystal XRD and GIWAXS.

n	**Parameter**	**Single Crystal**	**GIWAXS**
3	a (Å)	9.9846(9)	9.4±0.2
	b (Å)	15.2085(3)	11.5±0.2
	c (Å)	15.4812(6)	14.0±0.2
	α (°)	101.680(3)	88.5±0.3
	β (°)	95.697(3)	85.0±0.3
	γ (°)	108.613(3)	94.5±0.3
4	a (Å)	9.7669(7)	10.1±0.2
	b (Å)	15.3758(11)	12.4±0.2
	c (Å)	17.3850(12)	16.1±0.2
	α (°)	73.683(2)	88.0±0.3
	β (°)	85.076(2)	88.5±0.3
	γ (°)	71.659(2)	86.5±0.3
5	a (Å)	10.0750(4)	10.2±0.2
	b (Å)	14.6460(5)	14.1±0.2
	c (Å)	15.6820(6)	16.5±0.2
	α (°)	82.593(3)	81.5±0.3
	β (°)	78.874(3)	88.0±0.3
	γ (°)	82.281(3)	86.5±0.3
6	a (Å)	X	10.4±0.2
	b (Å)	X	15.8±0.2
	c (Å)	X	17.0±0.2
	α (°)	X	85.5±0.3
	β (°)	X	90.0±0.3
	γ (°)	X	72.0±0.3

9. References

[S1] A. Laguerre, K. Hukezalie, P. Winckler, F. Katranji, G. Chanteloup, M. Pirrotta, J.-M. Perrier-Cornet, J. M. Y. Wong, D. Monchaud, *J. Am. Chem. Soc.* **2015**, *137*, 8521–8525.

[S2] S. Shinamura, I. Osaka, E. Miyazaki, A. Nakao, M. Yamagishi, J. Takeya, K. Takimiya, *J. Am. Chem. Soc.* **2011**, *133*, 5024–5035.

[S3] K. Sekine, J. Schulmeister, F. Paulus, K. P. Goetz, F. Rominger, M. Rudolph, J. Zaumseil**,** A. S. K. Hashmi, *Chem. Eur. J.* **2019**, *25*, 216.

[S4] H.H Choi, K. Cho, C. D. Frisbie, H. Sirringhaus, and V. Podzorov, *Nat.Mater.* **2018**, *17*, 2-7.